Exportin 1 inhibitor KPT-330 reverses oxaliplatin resistance via p53 nuclear retention in colorectal cancer

CHUANXI LAI[1,2*], XIYA JIA[1,2*], YIYI CHEN[1,2], KANGKE CHEN[1,2], FEI WANG[1,2], QIQI ZHANG[3], XIAONAN XIANG[1,2], ZHE-SHENG CHEN[4], LINGNA XU[1,2] and SHENG DAI[1,2]

[1]Department of Colorectal Surgery, Sir Run Run Shaw Hospital, School of Medicine, Zhejiang University, Hangzhou, Zhejiang 310016, P.R. China; [2]Key Laboratory of Biotherapy of Zhejiang Province, Hangzhou, Zhejiang 310016, P.R. China; [3]Bone Marrow Transplantation Center, The First Affiliated Hospital of Zhejiang University School of Medicine, Hangzhou, Zhejiang 310006, P.R. China; [4]Department of Pharmaceutical Sciences, College of Pharmacy and Health Sciences, St. John's University, Queens, NY 11439, USA

Received May 16, 2025; Accepted August 13, 2025

DOI: 10.3892/ijmm.2025.5675

Abstract. Despite the established clinical efficacy of oxaliplatin in colorectal cancer (CRC), resistance to this platinum-based agent continues to pose a significant therapeutic challenge. Increased exportin 1 (XPO1) expression in CRC has been linked to chemoresistance, while KPT-330, a selective XPO1 inhibitor, has exhibited potential in enhancing platinum drug effectiveness in other cancer types. The present study explored the synergistic effects of KPT-330 and oxaliplatin in oxaliplatin-resistant CRC models. Oxaliplatin-resistant cell lines (HCT116/L-OHP and HCT8/L-OHP) were developed, exhibiting elevated XPO1 expression as demonstrated by western blotting. A range of *in vitro* assays (Cell Counting Kit-8 assays, ethynyldeoxyuridine assays, crystal violet staining, transmission electron microscopy and flow cytometry) and an *in vivo* subcutaneous xenograft model in nude mice were used to evaluate the combination therapy. Co-treatment with KPT-330 and oxaliplatin induced G_2/M phase arrest and mitochondrial dysfunction, thereby triggering apoptosis and ferroptosis. Mechanistically, the combination therapy of KPT-330 and oxaliplatin promoted the nuclear retention of p53, which in turn upregulated p21 and downregulated solute carrier family 7 member 11. *In vivo*, the combination therapy significantly enhanced tumor sensitivity to oxaliplatin. These results suggested that KPT-330 restored oxaliplatin sensitivity in resistant CRC by facilitating p53 nuclear retention, presenting a promising approach to overcome chemoresistance through dual modulation of cell cycle arrest and ferroptosis pathways.

Correspondence to: Dr Sheng Dai or Dr Lingna Xu, Department of Colorectal Surgery, Sir Run Run Shaw Hospital, School of Medicine, Zhejiang University, 3 Qingchun East Road, Shangcheng, Hangzhou, Zhejiang 310016, P.R. China
E-mail: daimd@zju.edu.cn
E-mail: xulingna@zju.edu.cn

*Contributed equally

Key words: KPT-330, oxaliplatin resistance, p53, colorectal cancer, combination therapy

Introduction

Colorectal cancer (CRC) is an aggressive malignancy, ranking third and second globally in terms of morbidity and mortality rates, respectively (1). The incidence of CRC in China is also rising steadily (2). The primary treatment approach for CRC combines surgery with chemotherapy and radiotherapy; however, not all patients respond to these standard therapies (3). Despite ongoing advancements in combined treatment strategies, including surgery, radiotherapy, chemotherapy, targeted therapy and immunotherapy, the survival rate of CRC remains suboptimal, with a high recurrence rate (3,4).

Oxaliplatin, a third-generation cisplatin analog, is widely used in CRC treatment (5). While the 5-fluorouracil, folinic acid and oxaliplatin regimen is initially effective, ~50% of patients with stage II and III CRC develop resistance to oxaliplatin-based adjuvant therapy (6). Previous studies have identified several mechanisms of oxaliplatin resistance, including anti-apoptotic signaling, ferroptosis, DNA repair, autophagy and altered drug transport (7,8). However, the precise mechanisms underlying oxaliplatin resistance remain unclear.

KPT-330, a selective exportin 1 (XPO1) inhibitor, has shown marked efficacy in tumor treatment (9,10). Ferreiro-Neira *et al* (11) demonstrated that KPT-330 enhances the sensitivity of CRC to radiotherapy, suggesting a potential novel therapeutic model, the combination therapy with KPT-330 and radiotherapy. A separate report has indicated that sequential administration of XPO1 and an ataxia telangiectasia and Rad3-related protein inhibitor (AZD-6738) improved therapeutic outcomes in TP53-mutated CRC (12). Additionally, KPT-330 has been found to enhance the efficacy of platinum-based chemotherapy in lung and ovarian cancer (13,14). However, to the best of our knowledge, no studies have explored the relationship between KPT-330 and oxaliplatin resistance in CRC. Thus, the combination of oxaliplatin and KPT-330 warrants investigation as a potential strategy for overcoming resistance in CRC, with further exploration of its underlying mechanisms.

We hypothesized that KPT-330 could restore oxaliplatin sensitivity in resistant CRC cells. To test this hypothesis, the present study aimed to systematically evaluate the therapeutic potential of KPT-330 in combination with oxaliplatin in oxaliplatin-resistant CRC cells. The present investigation focused on the underlying mechanisms of this combination regimen. Changes in the mitochondrial membrane potential (MMP) were monitored to assess mitochondrial function, and the effects on cell death pathways, including apoptosis and ferroptosis, were investigated. Furthermore, the present study examined the role of key molecular players by analyzing p53 nuclear translocation, p21 expression and the expression of the ferroptosis-related gene solute carrier family 7 member 11 (SLC7A11). Finally, a subcutaneous xenograft model was established to evaluate the *in vivo* efficacy of this combination regimen.

Materials and methods

Reagents and antibodies. HCT116 (cat. no. CCL-247), HCT8 (cat. no. CCL-244) and FHC (cat. no. CRL-1831) cell lines were obtained from American Type Culture Collection. The β-actin (cat. no. 4967S), GAPDH (cat. no. 2118), p21 (cat. no. 2947), cleaved poly (ADP-ribose) polymerase (PARP) (cat. no. 5625T), cleaved caspase-3 (cat. no. 9664L), Bax (cat. no. 5023T), PARP (cat. no. 9532S), caspase-3 (cat. no. 9668S) and Bcl-2 (cat. no. 15071T) antibodies were sourced from Cell Signaling Technology, Inc. CDK1 (cat. no. A11420), cyclin B1 (CCNB1; cat. no. A19037), XPO1 (cat. no. A0299), glutathione peroxidase 4 (GPX4; cat. no. A11243) and SLC7A11 (cat. no. A2413) antibodies were obtained from ABclonal Biotech Co., Ltd. The Lamin B1 (cat. no. AF5161) antibody was obtained from Affinity Biosciences, Ltd. The p53 (cat. no. sc-126) and Ki67 (cat. no. sc-23900) antibodies were purchased from Santa Cruz Biotechnology, Inc. HRP-conjugated secondary antibodies (cat. nos. ZB-2306 and ZB-2305) were obtained from Beijing Zhongshan Jinqiao Biotechnology Co., Ltd.

Cell culture. All cells were cultured in a 37˚C incubator with 5% CO_2. The oxaliplatin-resistant HCT116 and HCT8 cell lines (HCT8/L-OHP and HCT116/L-OHP) were developed by progressively increasing oxaliplatin concentrations, starting at 2 μM and reaching a final concentration of 14 μM, over a period of ≥9 months. HCT8, HCT8/L-OHP and HCT116/L-OHP cells were cultured in RPMI-1640 medium (cat. no. CR-31800; Cienry Co., Ltd.) supplemented with 10% fetal bovine serum (cat. no. BC-SE-FBS01C; Bio-Channel Biotechnology Co., Ltd.) and 10,000 U/ml penicillin-streptomycin (cat. no. ant-pm-05; InvivoGen). The HCT116 cell line was cultured in McCoy's 5A medium (cat. no. CR-16600; Cienry Co., Ltd.) with 10% fetal bovine serum and 10,000 U/ml penicillin-streptomycin, while FHC cells were cultured in DMEM (cat. no. CR-12800; Cienry Co., Ltd.) with 10% fetal bovine serum and 10,000 U/ml penicillin-streptomycin.

Cell viability test. For cell viability assays, $5x10^3$ cells per well were plated on 96-well plates and treated with different drugs at 37˚C for 48 h. For single-agent dose-response curves, cells were treated with oxaliplatin (0.33, 1, 3.3, 10, 33 and 100 μM; cat. no. HY-17371; MedChemExpress) or KPT-330 (0.001, 0.003, 0.01, 0.03, 0.1, 0.3, 1 and 3 μM; cat. no. S7252; Selleck Chemicals). For two-agent dose-response curves, cells were treated with a combination of oxaliplatin (0.33, 1, 3.3, 10, 33 and 100 μM) and KPT-330 (10 and 33 nM). After silencing of XPO1, cells were treated with oxaliplatin (0.5, 1, 2, 4, 8, 16 and 32 μM). For experiments involving combination therapy and specific inhibitors, the following treatments were performed on HCT116/L-OHP and HCT8/L-OHP cells: Cells were treated with single agents, including oxaliplatin (10 μM) and KPT-330 (33 nM), as well as their combination. For inhibitor assays, a combination of oxaliplatin (10 μM) and KPT-330 (33 nM) was used along with either Z-VAD-FMK (10 μM; cat. no. HY-16658B; MedChemExpress) or Fer-1 (1 μM; cat. no. HY-100579; MedChemExpress). Separately, oxaliplatin (2, 10 and 40 μM) was used to treat CRC (HCT8, HCT116, HCT116/L-OHP and HCT8/L-OHP cells) and normal cells (FHC cells). Cell viability was then assessed using the Cell Counting Kit-8 (cat. no. MA0218; Dalian Meilun Biology Technology Co., Ltd.). Cells were incubated with Cell Counting Kit-8 solution at 37˚C for 2 h according to the manufacturer's instructions.

Annexin V and PI staining. Apoptosis was detected using the Annexin V-FITC/PI kit [cat. no. AT101C; MultiSciences (Lianke) Biotech Co., Ltd.]. Following treatment with different drugs (oxaliplatin, 10 μM; KPT-330, 33 nM; Z-VAD-FMK, 10 μM) at 37˚C for 48 h, cells were harvested and stained with annexin V and PI for 15 min, and analyzed by flow cytometry (Fortessa; BD Biosciences). Apoptotic cells were quantified as the sum of early apoptotic cells (annexin V^+/PI^-) in the lower-right quadrant and late apoptotic cells (annexin V^+/PI^+) in the upper-right quadrant. Data were analyzed using FlowJo software (version 10.8; BD Biosciences).

Cell cycle assay. For cell cycle analysis, $2x10^5$ cells per well were seeded on 6-well plates and cultured for 24 h in serum-free medium until they reached 30-40% confluence. Cells were then treated with drugs (oxaliplatin, 10 μM; KPT-330, 33 nM; or the combination) for 48 h at 37˚C in a CO_2 incubator. In a separate experiment, HCT116 and HCT116/L-OHP cells were treated with oxaliplatin (2 μM) for 48 h at 37˚C. After treatment, cells were harvested, stained using the Cell Cycle Staining Kit [cat. no. CCS012; MultiSciences (Lianke) Biotech Co., Ltd.] for 15 min at room temperature in the dark, and analyzed by flow cytometry (Fortessa; BD Biosciences). Data were analyzed using FlowJo software (version 10.8; BD Biosciences).

Reactive oxygen species (ROS) assay. Cells ($2x10^5$ per well) were seeded on 6-well plates and cultured until they reached 30-40% confluence. The cells were then treated with drugs (oxaliplatin, 10 μM; KPT-330, 33 nM; or the combination) for 48 h at 37˚C in a CO_2 incubator. In a separate experiment, HCT116 and HCT116/L-OHP cells were treated with oxaliplatin (2 μM) for 48 h at 37˚C. After treatment, the cells were incubated in serum-free medium containing 2',7'-dichlorodihydrofluorescein diacetate (cat. no. S0033; Beyotime Institute of Biotechnology), MitoSOX Red (cat. no. HY-D1055; MedChemExpress), a fluorescent probe specifically designed for the detection of mitochondrial superoxide, or the

C11-BODIPY probe (cat. no. D3861; Invitrogen; Thermo Fisher Scientific, Inc.), a fluorescent probe for the detection of lipid peroxidation in cells, at 37˚C for 20 min. Following incubation, the fluorescence intensity was measured by flow cytometry (CytoFLEX; Beckman Coulter, Inc.). Data were analyzed using FlowJo software (version 10.8; BD Biosciences).

Measurement of malondialdehyde (MDA) levels. Cells ($2x10^5$ per well) were seeded into 6-cm dishes and cultured overnight. After 48 h of drug treatment (oxaliplatin, 10 μM; KPT-330, 33 nM; or the combination) at 37˚C, cells were harvested and lysed. The BCA Protein Assay Kit (cat. no. P0012; Beyotime Institute of Biotechnology) was used to quantify the protein concentration. Following protein quantification, MDA (cat. no. S0131S; Beyotime Institute of Biotechnology) working solution was added to the lysate, and the mixture was heated at 100˚C for 15 min. After centrifugation at 1,000 x g for 10 min at room temperature, the supernatant was collected and its absorbance was measured at 532 nm using a microplate reader.

Measurement of glutathione (GSH) levels. Cells ($2x10^5$ per well) were seeded into 6-cm dishes and cultured overnight. After 48 h of drug treatment (oxaliplatin, 10 μM; KPT-330, 33 nM; or the combination) at 37˚C, cells were harvested, processed according to the GSH and GSSG Assay Kit instructions (cat. no. S0053; Beyotime Institute of Biotechnology), and the absorbance was finally measured spectrophotometrically at a wavelength of 412 nm.

Measurement of the MMP. Cells ($2x10^5$ per well) were seeded on 6-well plates and cultured overnight. After 48 h of drug treatment (oxaliplatin, 10 μM; KPT-330, 33 nM; or their combination) at 37˚C in a CO_2 incubator, the treated cells were incubated with 1 ml JC-1 staining buffer (cat. no. C2006; Beyotime Institute of Biotechnology) for 20 min at 37˚C in the dark. In a separate experiment, HCT116 and HCT116/L-OHP cells were also treated with oxaliplatin (2 μM) for 48 h at 37˚C and then stained with 1 ml JC-1 staining buffer for 20 min at 37˚C in the dark. After incubation, the supernatant was removed, and cells were centrifuged at 600 x g for 4 min at 4˚C. The cells were then washed twice with JC-1 washing buffer (1X) and resuspended in the washing buffer. JC-1 fluorescence was assessed by flow cytometry (Fortessa; BD Biosciences). Data were analyzed using FlowJo software (version 10.8; BD Biosciences).

Xenograft tumor model. All animal procedures were approved by the Ethical Review Committee and Laboratory Animal Welfare Committee of the Sir Run Run Shaw Hospital, Zhejiang University School of Medicine (approval no. SRRSH2025-0023; Hangzhou, China). The experimental mice were purchased from Hangzhou Ziyuan Laboratory Animal Technology Co., Ltd. A total of 20 female BALB/c nude mice (16-18 g; 6 weeks old) were used in the present study. The mice were housed in a standard specific-pathogen-free environment for 1 week before the experiment for acclimation. Housing conditions were maintained at 22±2˚C and 55±10% humidity, with a 12/12 h light/dark cycle (7:00-19:00), with free access to food and sterile water.

For tumor implantation, $2x10^6$ HCT116/L-OHP cells suspended in 100 μl PBS were subcutaneously injected into the right flank of each mouse. After 1 week, the mice were randomly assigned to four treatment groups (5 mice per group): Vehicle control (5% DMSO, 40% PEG300, 5% Tween 80 and 50% ddH_2O; once per week), oxaliplatin (cat. no. HY-17371; MedChemExpress) alone (10 mg/kg; once per week), KPT-330 (cat. no. S7252; Selleck Chemicals) alone (10 mg/kg; once per week), or a combination of oxaliplatin and KPT-330.

Tumor size was measured with Vernier calipers on the indicated days following the start of treatment: Days 1, 3, 5, 8, 10, 12, 15, 17, 20, 22, 24, 27 and 29. The total time interval from injection to final tumor measurement was 35 days. Euthanasia was performed at the end of the pre-defined 4-week treatment period. At that time, the maximum tumor diameter was 16.8 mm, and the maximum tumor volume was 1,209.6 mm^3. Euthanasia was performed by gradually filling a chamber with CO_2 at a displacement rate of 35% of the chamber volume per min, with exposure for ≥5 min after visible cessation of respiration. Death was confirmed by the loss of respiration, loss of muscle tone and subsequent cervical dislocation after CO_2 inhalation. Tumors were dissected and embedded in paraffin on day 29 after the start of treatment. The tumor volume was calculated using the following formula: Tumor volume (mm^3)=tumor length x tumor $width^2/2$.

Transmission electron microscopy (TEM). Before being fixed for TEM, HCT116/L-OHP cells were treated with oxaliplatin (10 μM), KPT-330 (33 nM) or a combination of both. In a separate experiment, HCT116 and HCT116/L-OHP cells were treated with oxaliplatin (2 μM). All treatments were performed for 48 h at 37˚C. Experimental cells were fixed with 2.5% glutaraldehyde in 0.1 M sodium cacodylate buffer (pH 7.4) for 2 h at 25˚C, and then stored at 4˚C in the same fixative overnight. After three washes with PBS, the samples were incubated in 1% osmium tetroxide for 1 h at room temperature, followed by three washes with water. The samples were then incubated in 2% uranyl acetate for 30 min at room temperature. After dehydration through a series of ethanol steps (15 min each in 50, 70, 90 and 100% ethanol) and two 20-min washes in 100% acetone, the samples were embedded in epoxy resin for 24 h at 60˚C and sectioned into ultrathin slices (90 nm). The sections were imaged using a Tecnai G2 Spirit 120kV transmission electron microscope (FEI; Thermo Fisher Scientific, Inc.).

Immunohistochemistry (IHC) assay. The tissues were fixed in 4% paraformaldehyde overnight at 4˚C, followed by dehydration, clearing and paraffin embedding. The paraffin sections (5 μm) were then baked at 60˚C for 2 h, deparaffinized in xylene and rehydrated through a descending series of graded alcohols. Antigen retrieval was carried out using sodium citrate buffer for 10 min at 100˚C. Endogenous peroxidase activity was blocked with 3% H_2O_2 for 10 min at room temperature. Non-specific binding was blocked with 10% goat serum (cat. no. SL038; Beijing Solarbio Science & Technology Co., Ltd.) for 30 min at room temperature. The sections were then incubated with primary antibodies against Ki67 (1:1,000; cat. no. sc-23900; Santa Cruz Biotechnology, Inc.)

or p53 (1:1,000; cat. no. sc-126; Santa Cruz Biotechnology, Inc.) overnight at 4˚C. After washing, the sections were incubated with an HRP-conjugated goat anti-mouse IgG (1:5,000; ZB-2305; Beijing Zhongshan Jinqiao Biotechnology Co., Ltd.) secondary antibody for 1 h at 37˚C. Color was developed with a DAB kit (cat. no. ZLI-9017; Beijing Zhongshan Jinqiao Biotechnology Co., Ltd.) for 30 sec at room temperature, and the sections were counterstained with hematoxylin for 1 min at room temperature before being mounted and observed under a light microscope (Whole Slide Scanning System; Olympus VS200; Olympus Corporation). To evaluate the percentage of Ki67-positive nuclei, five fields per group were randomly selected and a total of 1,000 cells were counted. The Ki67 proliferation index was calculated as the percentage of Ki67-positive nuclei out of the total number of cells counted.

Reverse transcription-quantitative PCR (RT-qPCR) analysis of mRNA expression. Total RNA from treated cells was extracted using the AG RNAex Pro Reagent (cat. no. AG21101; Hunan Accurate Bio-Medical Technology Co., Ltd.) and the SteadyPure RNA Extraction Kit (cat. no. AG21024; Hunan Accurate Bio-Medical Technology Co., Ltd.). Prior to RNA extraction, cells were treated with oxaliplatin (10 μM), KPT-330 (33 nM) or a combination of both for 48 h at 37˚C. RNA (~1.0 μg) was reverse-transcribed to generate the first strand of cDNA using the Evo M-MLV RT Mix Kit with gDNA Clean for qPCR Ver.2 (cat. no. AG11728; Hunan Accurate Bio-Medical Technology Co., Ltd.). The reverse transcription reaction was performed at 37˚C for 15 min, followed by heating at 85˚C for 5 sec. qPCR was performed using ChamQ Universal SYBR qPCR Master Mix (cat. no. Q711-02; Vazyme Biotech Co., Ltd.). The thermocycling conditions were as follows: Initial denaturation at 95˚C for 30 sec, followed by 40 cycles of 95˚C for 10 sec (denaturation) and 60˚C for 30 sec (annealing/extension). GAPDH was used as the internal reference gene. The relative gene expression levels were quantified using the $2^{-\Delta\Delta Cq}$ method (15). The primer pairs used for qPCR were as follows: GAPDH forward, 5'-GGAGCGAGATCC CTCCAAAAT-3' and reverse, 5'-GGCTGTTGTCATACT TCTCATGG-3'; CDK1 forward, 5'-AAACTACAGGTCAAG TGGTAGCC-3' and reverse, 5'-TCCTGCATAAGCACA TCCTGA-3'; CCNB1 forward, 5'-AATAAGGCGAAGATC AACATGGC-3' and reverse, 5'-TTTGTTACCAATGTCCCC AAGAG-3'; SLC7A11 forward, 5'-TCTCCAAAGGAGGTT ACCTGC-3' and reverse, 5'-AGACTCCCCTCAGTAAAGT GAC-3'; and GPX4 forward, 5'-ACAAGAACGGCTGCG TGGTGAA-3' and reverse, 5'-GCCACACACTTGTGGAGCT AGA-3'.

Western blot analysis. Treated cells and tissues were washed 2-3 times with PBS, then lysed using RIPA buffer (cat. no. P0013B; Beyotime Institute of Biotechnology). Prior to protein analysis, HCT8, HCT116, HCT116/L-OHP and HCT8/L-OHP cells were treated with a range of oxaliplatin concentrations (1, 2, 4, 8 and 16 μM). HCT116/L-OHP and HCT8/L-OHP cells were also treated with a series of KPT-330 concentrations (10, 33, 100, 333 and 1,000 nM). HCT116/L-OHP and HCT8/L-OHP cells were treated with oxaliplatin (10 μM), KPT-330 (33 nM) or a combination of both. Additionally, after silencing of p53, HCT116/L-OHP cells were treated with oxaliplatin (10 μM), KPT-330 (33 nM) or a combination of both. All cell treatments were conducted for 48 h at 37˚C. The lysates were centrifuged at 12,000 x g for 15 min at 4˚C to collect the protein. Protein concentrations were quantified using a BCA assay (cat. no. MA0082-2; Dalian Meilun Biology Technology Co., Ltd.). Proteins (20 μg/lane) were separated by 10% SDS-PAGE and transferred onto PVDF membranes (cat. no. ISEQ00010; Sigma-Aldrich; Merck KGaA). The membranes were blocked with 5% BSA (cat. no. 9048-46-8; Dalian Meilun Biology Technology Co., Ltd.) for 1 h at room temperature, and incubated with the specified primary antibodies specific to the target proteins β-ACTIN (cat. no. 4967S), GAPDH (cat. no. 2118), p21 (cat. no. 2947), cleaved PARP (cat. no. 5625T), cleaved caspase-3 (cat. no. 9664L), Bax (cat. no. 5023T), PARP (cat. no. 9532S), caspase-3 (cat. no. 9668S), Bcl-2 (cat. no. 15071T), CDK1 (cat. no. A11420), CCNB1 (cat. no. A19037), XPO1 (cat. no. A0299), GPX4 (cat. no. A11243), SLC7A11 (cat. no. A2413), Lamin B1 (cat. no. AF5161) and p53 (cat. no. sc-126), all at a dilution of 1:1,000, overnight at 4˚C. Afterwards, the membranes were washed three times with PBS and incubated with the appropriate HRP-conjugated secondary antibodies (cat. nos. ZB-2306 and ZB-2305; 1:10,000) for 1 h at room temperature. Protein bands were visualized using an FDbio-Dura ECL kit (cat. no. FD8020; Hangzhou Fude Biological Technology Co., Ltd.), and semi-quantified using ImageJ analysis software (version 8; National Institutes of Health).

A fractionation assay [HCT8/L-OHP and HCT116/L-OHP cells were treated with oxaliplatin (10 μM), KPT-330 (33 nM) or a combination of both for 48 h at 37˚C] was performed to obtain nuclear and cytoplasmic protein fractions using the Nuclear and Cytoplasmic Protein Extraction Kit (cat. no. P0028B; Beyotime Institute of Biotechnology) according to the manufacturer's instructions. The separated fractions were then subjected to western blotting as aforementioned.

Immunofluorescence analysis. HCT116/L-OHP and HCT8/L-OHP cells ($5x10^4$ per well) were seeded in confocal culture dishes (cat. no. 801001; Wuxi NEST Biotechnology Co., Ltd.) and cultured overnight. The cells were then treated with oxaliplatin (10 μM), KPT-330 (33 nM) or a combination of both for 48 h at 37˚C. Following treatment, the cells were fixed with 4% paraformaldehyde overnight at 4˚C, permeabilized with 0.1% Triton X-100 at room temperature for 15 min and blocked with 10% goat serum (cat. no. MB4508-1; Dalian Meilun Biology Technology Co., Ltd.) at room temperature for 1 h. After blocking, cells were incubated with a mouse anti-p53 antibody (cat. no. sc-126; 1:500; Santa Cruz Biotechnology, Inc.) at 4˚C overnight. The cells were then incubated with a goat anti-mouse secondary antibody (cat. no. A-11001; Alexa Fluor 488; Thermo Fisher Scientific, Inc.) for 1 h at room temperature. Finally, the cells were stained with DAPI (1 mg/ml; cat. no. D3571; Thermo Fisher Scientific, Inc.) for 5 min at room temperature to visualize the nuclei, and images were captured using a laser scanning confocal fluorescence microscope. The fractional area of p53 in the nucleus was quantified by analyzing 10 cells from each treatment group, and was analyzed using ImageJ analysis software (version 8; National Institutes of Health).

Cell transfection. The target sequences of small interfering RNAs (siRNAs; Table SI) were synthesized by Suzhou GenePharma Co., Ltd. For transient transfection, Lipofectamine RNAiMAX (cat. no. 13778030; Thermo Fisher Scientific, Inc.) was used according to the manufacturer's protocol. A total of 5 μl of si-RNA (20 μM), 100 μl Opti-MEM (cat. no. CR22600; Cienry Co., Ltd.) and 6 μl Lipofectamine RNAiMAX were mixed at room temperature for 20 min. This complex was then added to 0.9 ml RPMI-1640 medium (resulting in a final siRNA concentration of 100 nM), and the cells were transfected for 8 h at 37˚C. After transfection, cells were allowed to recover for 24 h at 37˚C before being used in subsequent experiments. The transfection efficiency was determined by western blot analysis.

Ethynyldeoxyuridine (EdU) assay. Cell proliferation was assessed using an EdU assay kit (cat. no. C10310; Guangzhou RiboBio Co., Ltd.). Cells ($1x10^5$ per well) were seeded on 12-well plates and cultured overnight. After 48 h of drug treatment (oxaliplatin, 10 μM; KPT-330, 33 nM; or the combination) at 37˚C, cells were incubated with EdU at a final concentration of 50 μM for 2 h at 37˚C. The cells were then fixed, permeabilized and stained according to the manufacturer's instructions of the EdU assay kit. Finally, the images were captured using a laser scanning confocal fluorescence microscope.

Crystal violet assay. Cells ($1x10^5$ per well) were seeded on 12-well plates. When the cells reached 30-40% confluence, they were treated with oxaliplatin (5 or 10 μM), KPT-330 (10 or 33 nM) or a combination of the two (KPT-330 at 10 or 33 nM with oxaliplatin at 5 or 10 μM) for 48 h at 37˚C in a CO_2 incubator. The cells were then washed three times with PBS and fixed with 4% paraformaldehyde at room temperature for 15 min. Afterwards, the cells were washed twice with PBS and stained with crystal violet at room temperature for 20 min. The cells were washed three times with water, and images were captured.

Statistical analysis. Data are presented as the mean ± SD of at least three independent biological replicates (n≥3). All statistical analyses were performed using GraphPad Prism 8.0 (Dotmatics). Differences among multiple groups were compared using one-way ANOVA. If the data met the assumption of homogeneity of variances, Tukey's Honestly Significant Difference post hoc test was used. If the assumption was violated, Welch's ANOVA with Dunnett's T3 post hoc test was performed. $P<0.05$ was considered to indicate a statistically significant difference.

Results

KPT-330 and oxaliplatin combined inhibit the proliferation of oxaliplatin-resistant CRC cells. Oxaliplatin-resistant cell lines were established using oxaliplatin-sensitive CRC cell lines (HCT116 and HCT8) (Fig. 1A). Notably, HCT116/L-OHP and HCT8/L-OHP cells exhibited higher IC_{50} values (45.94 μM for HCT116/L-OHP cells and 50.91 μM for HCT8/L-OHP cells) compared with their parental counterparts HCT116 (2.979 μM) and HCT8 (4.847 μM) cells (Fig. 1B). Previous research has suggested that XPO1 expression is negatively associated with the prognosis of patients with CRC, positioning XPO1 as a potential therapeutic target for CRC (16). Furthermore, KPT-185, a selective XPO1 inhibitor, synergistically induces apoptosis in human pancreatic and colon cancer cell lines when combined with oxaliplatin (17). In line with these findings, XPO1 expression was higher in the newly established oxaliplatin-resistant cell lines compared with their parental counterparts (Fig. S1A). Oxaliplatin treatment induced a concentration-dependent increase in XPO1 expression in both HCT116/L-OHP and HCT8/L-OHP cells (Fig. 1C). Additionally, a similar induction of XPO1 expression was observed in both HCT116 and HCT8 cells following oxaliplatin treatment (Fig. S1B).

The cytotoxic effects of oxaliplatin and KPT-330 were subsequently assessed *in vitro* using four CRC cell lines (HCT8, HCT8/L-OHP, HCT116 and HCT116/L-OHP) and the non-cancerous FHC cells. Low concentrations of oxaliplatin decreased the viability of sensitive CRC cells, whereas high concentrations of oxaliplatin decreased the viability of FHC cells. The inhibitory effect on resistant CRC cells was less pronounced than that on sensitive CRC cells and FHC cells (Fig. 1D). The IC_{50} values for KPT-330 ranged between 0.1 and 0.3 μM in CRC cells, while 1.3 μM KPT-330 suppressed the viability of non-cancerous FHC cells (Fig. 1G). Silencing of XPO1 using two distinct siRNAs in HCT116/L-OHP and HCT8/L-OHP cells, which are resistant to oxaliplatin, enhanced their sensitivity to oxaliplatin (Fig. 1E and F). The inhibition of XPO1 expression by KPT-330 was found to be dose-dependent, and KPT-330 could enhance the sensitivity of oxaliplatin-resistant CRC cells to oxaliplatin by downregulating XPO1 expression (Fig. 1H-J). These results collectively demonstrated a synergistic effect of KPT-330 and oxaliplatin in overcoming resistance in CRC cells.

Combination of KPT-330 and oxaliplatin induces G_2/M cell cycle arrest in oxaliplatin-resistant CRC cells. In subsequent experiments, the combination treatment for 48 h resulted in a more significant reduction in the viability of HCT116/L-OHP and HCT8/L-OHP cells compared with oxaliplatin alone (Fig. 2A). EdU staining was employed to assess the impact of the KPT-330 and oxaliplatin combination on cell proliferation, revealing a pronounced inhibition of proliferation in both HCT116/L-OHP and HCT8/L-OHP cells following combined treatment (Fig. 2B). Oxaliplatin primarily induces G_2/M cell cycle arrest and a transient delay in the S phase (18). When comparing the cell cycle distribution of HCT116 and HCT116/L-OHP cells after 48 h of oxaliplatin (2 μM) treatment, a clear accumulation in the G_2/M phase was observed in HCT116 cells, accompanied by a reduction in cells in the S and G_0/G_1 phases (Fig. S2A). In HCT116/L-OHP cells, the combination treatment further reduced the proportion of cells in the S phase and notably increased the proportion of cells in the G_2/M phase compared with oxaliplatin (10 μM) alone (Fig. S2B and C). In HCT8/L-OHP cells, where oxaliplatin as a single agent had minimal effects, the combination therapy increased the proportion of cells in the G_2/M phase compared with oxaliplatin (10 μM) alone (Fig. S2B and C). These results suggested that KPT-330 and oxaliplatin influenced proteins associated with the G_2/M phase, as evidenced by the increase in the G_2/M cell population following combination

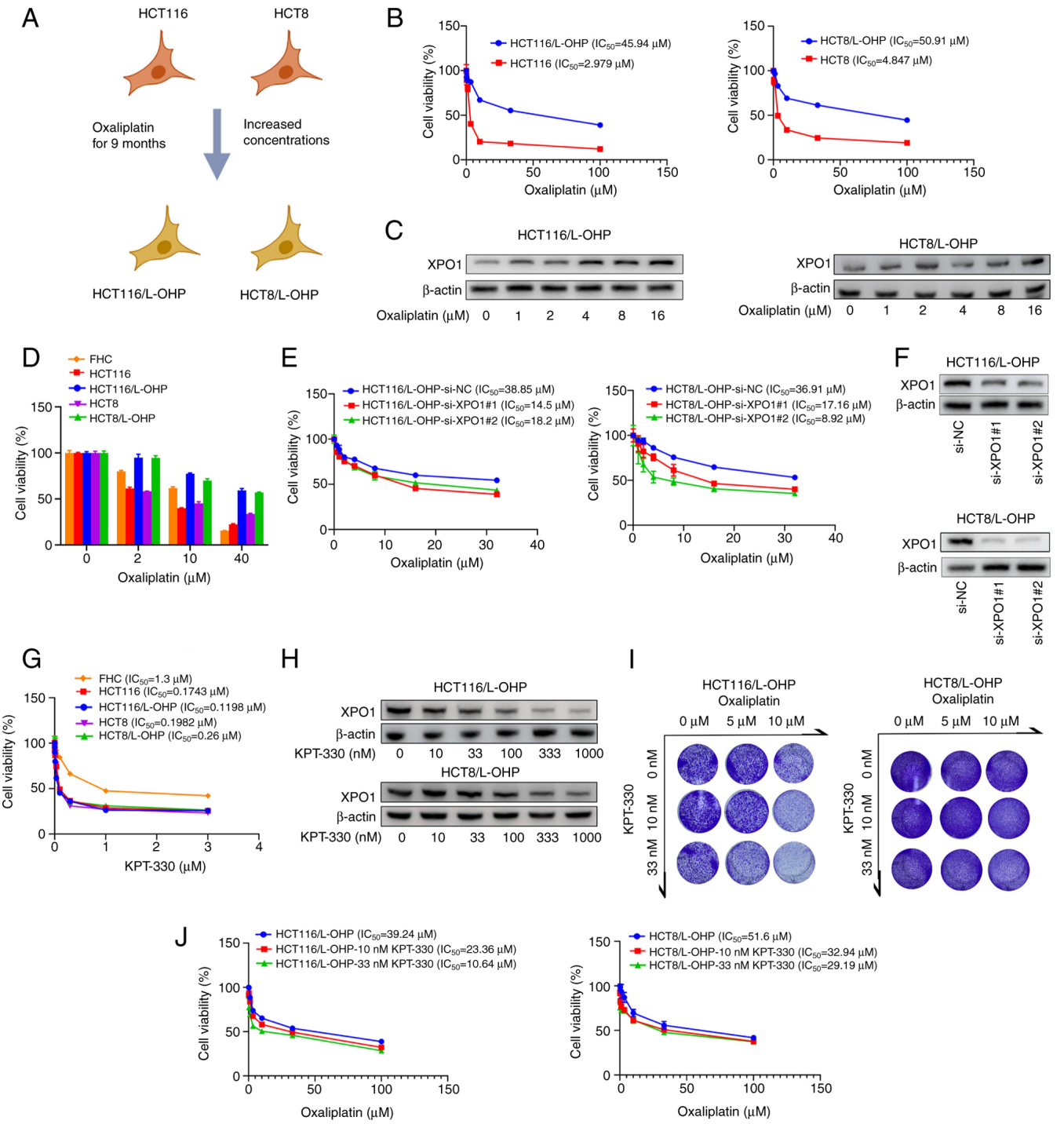

Figure 1. Combination of KPT-330 and oxaliplatin synergistically inhibits the viability of oxaliplatin-resistant CRC cells. (A) Schematic illustrating the process of constructing oxaliplatin-resistant HCT116/L-OHP and HCT8/L-OHP cell lines. (B) Dose-response curves for oxaliplatin in the four CRC cell lines, with cell viability measured using the CCK-8 assay after 48 h of treatment. (C) Immunoblot analysis of HCT116/L-OHP and HCT8/L-OHP cells treated with oxaliplatin for 48 h. (D) Viability of four CRC cell lines and FHC cells treated with oxaliplatin for 48 h, measured using a CCK-8 assay. (E) Viability of indicated cancer cell lines after silencing of XPO1 or transfection with si-NC, followed by 48 h of oxaliplatin treatment. (F) Immunoblot analysis of HCT116/L-OHP and HCT8/L-OHP cells after silencing of XPO1 or transfection with si-NC. (G) Dose-response curves for KPT-330 in the four CRC cell lines and FHC cells, with cell viability assessed using a CCK-8 assay after 48 h of treatment. (H) Immunoblot analysis of HCT116/L-OHP and HCT8/L-OHP cells treated with KPT-330 for 48 h. (I) Crystal violet assay for indicated cancer cell lines treated with different dosages of oxaliplatin and KPT-330. (J) Dose-response curves for oxaliplatin in the two CRC cell lines with a fixed dose of KPT-330, with cell viability measured using a CCK-8 assay after 48 h of treatment. CCK-8, Cell Counting Kit-8; CRC, colorectal cancer; NC, negative control; si, small interfering RNA; XPO1, exportin 1.

treatment. To explore the underlying mechanism of the cell cycle arrest induced by the combination, the expression of key G_2/M arrest markers was analyzed by western blotting. The protein and mRNA levels of CCNB1 and CDK1, which are critical regulators of the G_2/M phase, were reduced following combined treatment (Fig. 2D and E). Given the known role of p53 and p21 in modulating the CDK1-CCNB1 complex (19), the present results demonstrated that the combination treatment

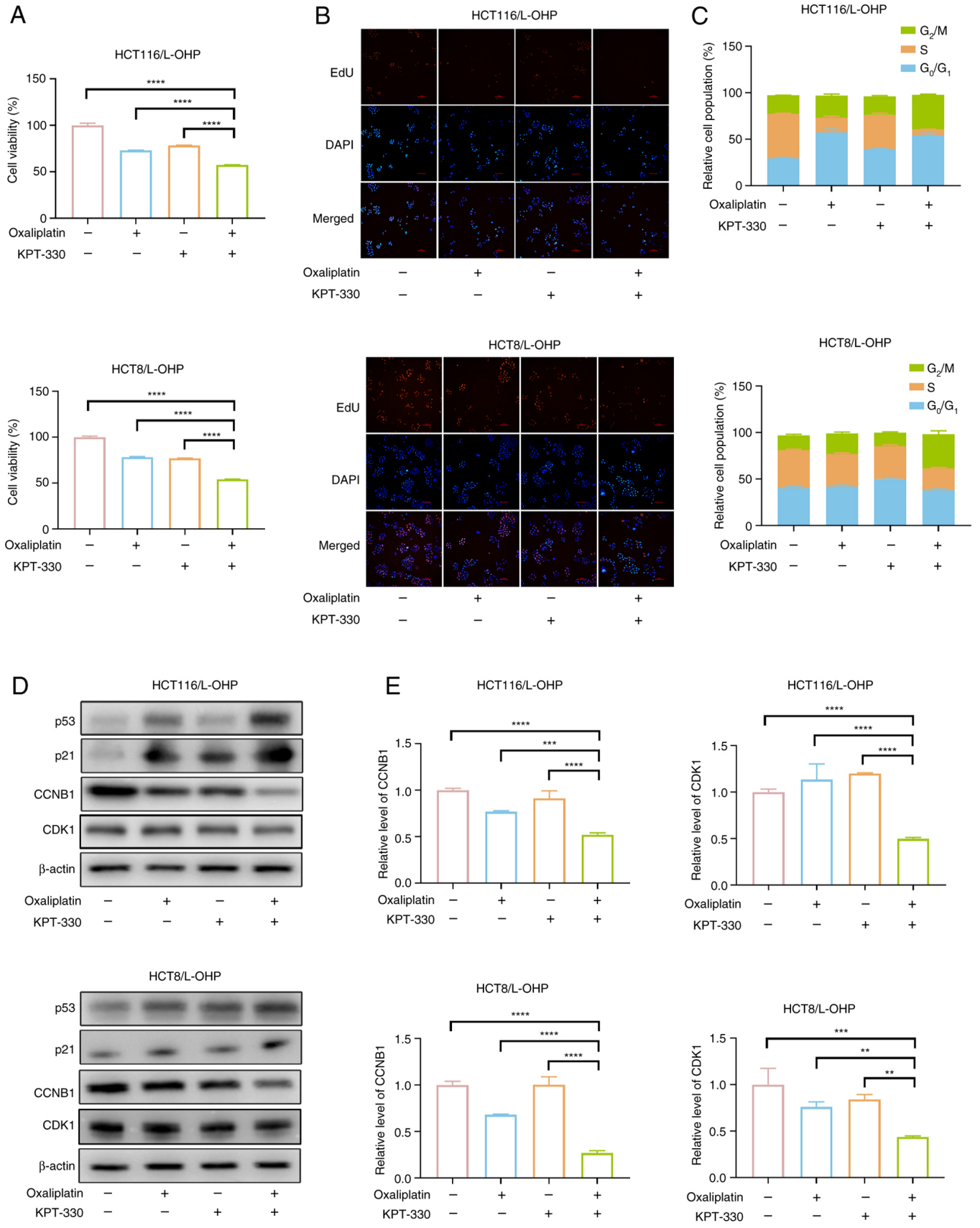

Figure 2. Combination of KPT-330 and oxaliplatin induces G_2/M cell cycle arrest in oxaliplatin-resistant colorectal cancer cells. (A) Viability of HCT116/L-OHP and HCT8/L-OHP cells treated with oxaliplatin, KPT-330 or the combination for 48 h, analyzed using a Cell Counting Kit-8 assay. (B) EdU proliferation analysis of HCT116/L-OHP and HCT8/L-OHP cells treated with oxaliplatin, KPT-330 or the combination for 48 h. Scale bar, 100 μm. (C) Cell cycle distribution detected by flow cytometry after 48 h of treatment with oxaliplatin, KPT-330 or the combination. (D) Immunoblot analysis of HCT116/L-OHP and HCT8/L-OHP cells treated with oxaliplatin, KPT-330 or the combination for 48 h. (E) mRNA expression levels of CCNB1 and CDK1 in HCT116/L-OHP and HCT8/L-OHP cells treated with oxaliplatin, KPT-330 or the combination for 48 h. **P<0.01; ***P<0.001; ****P<0.0001. CCNB1, cyclin B1; EdU, ethynyldeoxyuridine.

upregulated p53 and p21 protein expression, as evidenced by a subsequent downregulation of CDK1 and CCNB1 protein levels (Fig. 2D). These results collectively indicated that the KPT-330 and oxaliplatin combination induced G_2/M cell cycle arrest in oxaliplatin-resistant CRC cells.

Combination of KPT-330 and oxaliplatin induces apoptosis in oxaliplatin-resistant CRC cells. Compared with HCT116/L-OHP cells, oxaliplatin induced a significant increase in apoptosis in HCT116 cells (Fig. S3A), indicating that resistance to oxaliplatin in CRC is associated with anti-apoptotic mechanisms (20). To further explore whether the combination of oxaliplatin and KPT-330 synergistically induces apoptosis in oxaliplatin-resistant CRC cells, apoptosis levels were quantitatively assessed. While treatment with either oxaliplatin or KPT-330 alone did not significantly induce apoptosis in HCT116/L-OHP or HCT8/L-OHP cells, the combination therapy markedly enhanced apoptosis (Fig. 3A). To investigate whether the observed apoptosis was caspase-dependent, Z-VAD-FMK, a pan-caspase inhibitor, was employed (21,22). The results revealed that Z-VAD-FMK effectively blocked apoptosis induced by the combination therapy (Fig. 3B and C). Western blotting further demonstrated that oxaliplatin combined with KPT-330 increased cleaved PARP levels (Fig. 3D). Collectively, these results suggested that KPT-330 potentiated oxaliplatin-induced apoptosis in CRC cells.

Combination of KPT-330 and oxaliplatin increases the levels of ROS and induces mitochondrial dysfunction. Apoptosis is a multifaceted process involving caspase activation, MMP changes, the balance between pro-apoptotic and anti-apoptotic proteins, and other signaling pathways (23). Compared with HCT116/L-OHP cells, HCT116 cells exhibited greater sensitivity to oxaliplatin-induced changes in the MMP (Fig. S3B). To investigate whether the combination treatment induced apoptosis by affecting the MMP, JC-1, a fluorescent indicator of the MMP, was used. In both HCT116/L-OHP and HCT8/L-OHP cells, combination treatment with oxaliplatin and KPT-330 induced greater mitochondrial depolarization than monotherapy (Fig. 4A). However, in HCT8/L-OHP cells, low-dose KPT-330 treatment did not affect mitochondrial depolarization (Fig. 4A). Notably, the MMP loss in both KPT-330 and oxaliplatin monotherapy groups was lower than that of the control group. This finding suggests that while the single agents induced apoptosis, they might be triggering a different or less direct mitochondrial pathway in these resistant cells. Alternatively, the observed decrease in MMP loss could be a result of the adaptive mechanisms of the cells, which enables them to maintain mitochondrial function and viability under single-agent stress, thereby contributing to drug resistance. These results suggested that combination therapy may induce mitochondrial dysfunction. To further determine if this dysfunction is linked to increased ROS production, ROS levels were measured in the cells. Oxaliplatin treatment had a negligible effect on ROS induction in HCT116/L-OHP cells, in contrast to its marked effect on sensitive HCT116 cells (Fig. S3C), combination therapy increased ROS levels in both HCT116/L-OHP and HCT8/L-OHP cells (Fig. 4B). Given that most intracellular ROS are generated within mitochondria, the MitoSOX Red reagent, a mitochondria-targeted form of dihydroethidium, was used to examine mitochondrial ROS levels. The combination of oxaliplatin and KPT-330 further elevated mitochondrial ROS levels in both HCT116/L-OHP and HCT8/L-OHP cells compared with either monotherapy treatment (Fig. 4C). TEM images revealed morphological changes in the mitochondria following treatment with oxaliplatin, KPT-330 or the combination. Notably, the combination therapy resulted in increased membrane density and a shrunken mitochondrial morphology (Fig. 4D). Additionally, compared with those in HCT116/L-OHP cells, mitochondria in HCT116 cells displayed impaired morphology following oxaliplatin treatment (Fig. S3D). These results suggested that the combination of oxaliplatin and KPT-330 induced mitochondrial dysfunction through the elevation of ROS levels.

Combination of KPT-330 and oxaliplatin inhibits SLC7A11 and GPX4 expression to induce ferroptosis. The present TEM results (Fig. 4D) revealed that HCT116/L-OHP cells treated with combination therapy exhibited distinct morphological features characteristic of ferroptosis, an iron-dependent, non-apoptotic form of cell death marked by the accumulation of cytotoxic lipid ROS, leading to lipid membrane damage and perforation (24). Inducing ferroptosis can overcome oxaliplatin resistance in CRC cells (25,26). To further explore whether combination therapy sensitizes oxaliplatin-resistant cells to oxaliplatin by triggering ferroptosis, several experiments were conducted. Both lipid peroxidation and MDA levels were increased following combination treatment with oxaliplatin and KPT-330 (Fig. 5A and B). Inhibition of cell viability by the combination therapy was partially reversed using the ferroptosis inhibitor ferrostatin-1 (Fig. 5C). The present results demonstrated that combination therapy enhanced p53 expression. As a key regulator in tumorigenesis and development, p53 serves a critical role in both oxaliplatin resistance and ferroptosis (27). Based on this, it was hypothesized that combination therapy promotes p53 expression to activate ferroptosis-related signaling. Combination treatment reduced the mRNA and protein levels of SLC7A11 and GPX4 (Fig. 5D and E), and similarly decreased GSH levels (Fig. 5F). Knockdown of p53 partially counteracted the reduction in SLC7A11 and GPX4 expression induced by the combination therapy (Figs. S4 and 5G). These results indicated that the combination of KPT-330 and oxaliplatin induced ferroptosis by promoting p53 expression, which in turn suppressed SLC7A11 and GPX4 expression.

Combination of KPT-330 and oxaliplatin induces p53 nuclear retention. Combination treatment enhanced p53 expression. Given that XPO1 mediates the nuclear export of p53, the balance between its nuclear and cytoplasmic localization is a key mechanism that influences oxaliplatin sensitivity (28). Additionally, increased cytoplasmic p53 levels diminish cellular sensitivity to oxaliplatin (28,29). Cell fractionation experiments revealed that oxaliplatin monotherapy resulted in elevated p53 levels in both the cytoplasmic and nuclear fractions (Fig. 6A). Immunofluorescence analysis further demonstrated that oxaliplatin treatment alone notably promoted nuclear accumulation of p53 (Fig. 6A and B). In HCT116/L-OHP cells, combination therapy further enhanced nuclear p53 accumulation (Fig. 6A and B). In HCT8/L-OHP cells, the combination therapy not only reduced p53 nuclear export (Fig. 6A) but also

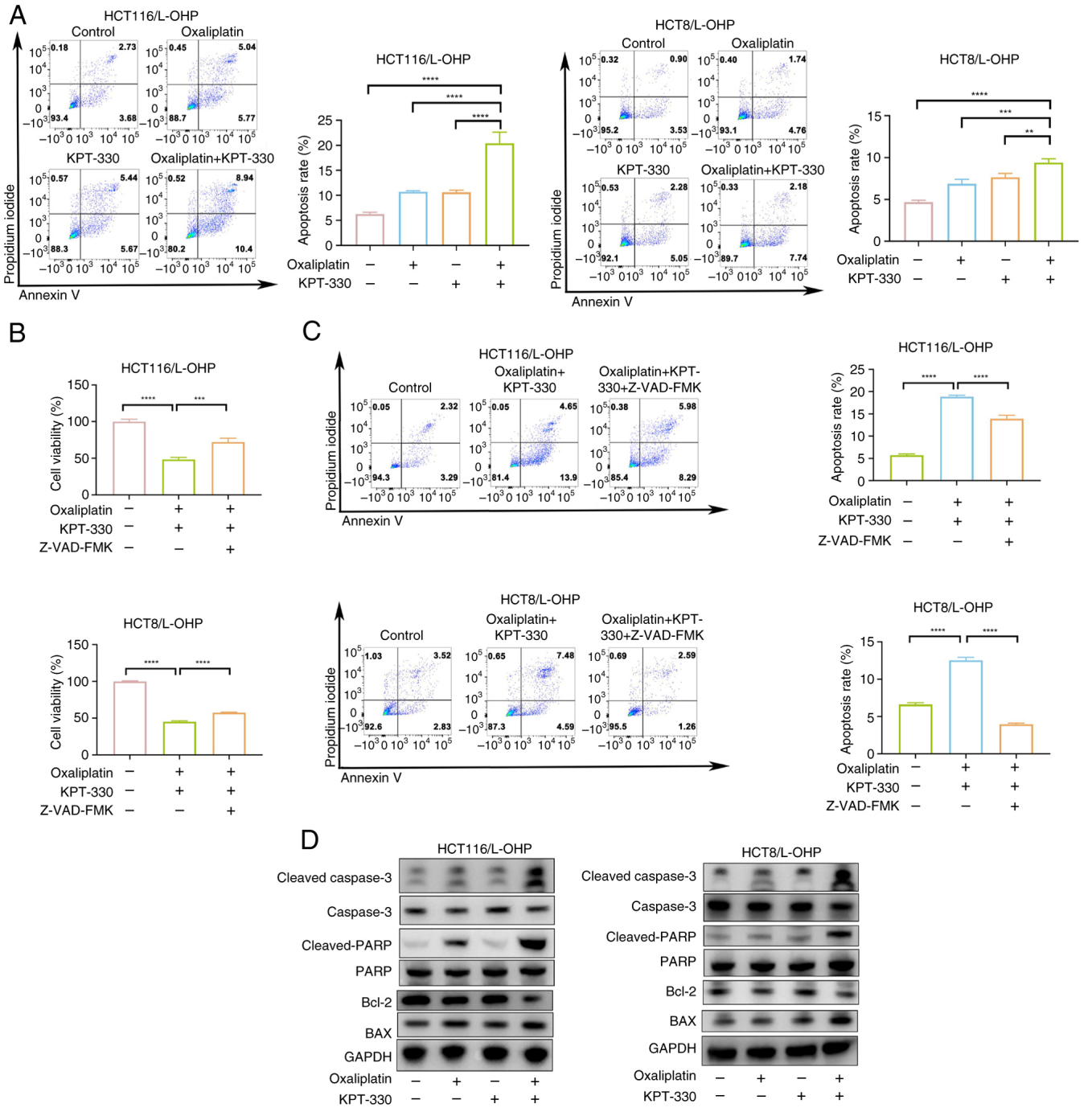

Figure 3. Combination of KPT-330 and oxaliplatin induces apoptosis in oxaliplatin-resistant colorectal cancer cells. (A) Apoptosis rate of HCT116/L-OHP and HCT8/L-OHP cells treated with oxaliplatin, KPT-330 or the combination for 48 h, assessed by flow cytometry. The sum of early apoptotic cells (annexin V^+/PI^-) in the lower-right quadrant and late apoptotic cells (annexin V^+/PI^+) in the upper-right quadrant indicates apoptotic cells, and was used for quantification. (B) Viability of HCT116/L-OHP and HCT8/L-OHP cells treated with oxaliplatin and KPT-330 or the combination with Z-VAD-FMK for 48 h, analyzed using a Cell Counting Kit-8 assay. (C) Apoptosis rate of HCT116/L-OHP and HCT8/L-OHP cells treated with oxaliplatin and KPT-330 or the combination with Z-VAD-FMK for 48 h, analyzed by flow cytometry. The sum of early apoptotic cells (annexin V^+/PI^-) in the lower-right quadrant and late apoptotic cells (annexin V^+/PI^+) in the upper-right quadrant indicates apoptotic cells, and was used for quantification. (D) Immunoblot analysis of HCT116/L-OHP and HCT8/L-OHP cells treated with oxaliplatin, KPT-330 or the combination for 48 h. $^{**}P<0.01$, $^{***}P<0.001$, $^{****}P<0.0001$. PARP, poly (ADP-ribose) polymerase.

increased nuclear p53 expression (Fig. 6A and B). In conclusion, these results indicated that the combination of KPT-330 and oxaliplatin induced p53 nuclear retention.

Combination of KPT-330 and oxaliplatin effectively suppresses tumor growth in a mouse xenograft model. Assessing the effectiveness of synergistic inhibition in animal models is crucial. A subcutaneous xenograft model was established by injecting HCT116/L-OHP cells subcutaneously. At 1 week after tumor implantation, four treatment groups were formed: Vehicle (once a week), oxaliplatin (10 mg/kg; once a week), KPT-330 (10 mg/kg; once a week) and combination treatment (Fig. 7A). After 4 weeks of treatment, the body weight of mice in the combination therapy

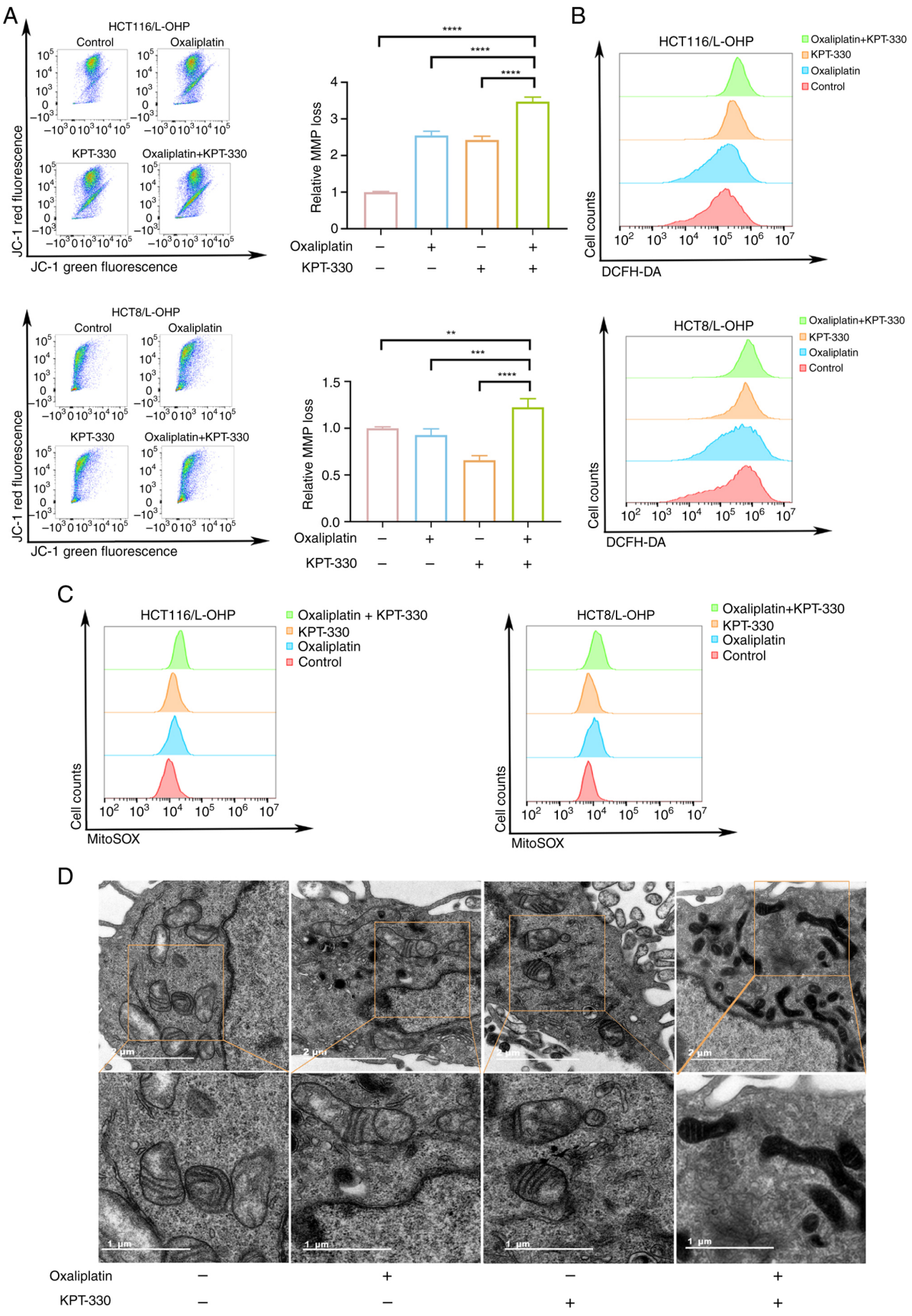

Figure 4. Combination of KPT-330 and oxaliplatin increases the levels of reactive oxygen species and induces mitochondrial dysfunction. (A) HCT116/L-OHP and HCT8/L-OHP cells were treated with oxaliplatin, KPT-330 or the combination for 48 h, stained with JC-1, and analyzed by flow cytometry. The bar chart shows the relative MMP loss in the four treatment groups. (B) HCT116/L-OHP and HCT8/L-OHP cells were treated with oxaliplatin, KPT-330 or the combination for 48 h, stained with DCFH-DA, and analyzed by flow cytometry. (C) HCT116/L-OHP and HCT8/L-OHP cells were treated with oxaliplatin, KPT-330 or the combination for 48 h, stained with MitoSOX, and analyzed by flow cytometry. (D) Representative transmission electron microscopy images of mitochondrial morphology in HCT116/L-OHP cells treated with oxaliplatin, KPT-330 or the combination for 48 h. Scale bars, 2 μm (upper panel) or 1 μm (lower panel). **P<0.01, ***P<0.001, ****P<0.0001. DCFH-DA, 2',7'-dichlorodihydrofluorescein diacetate; MMP, mitochondrial membrane potential.

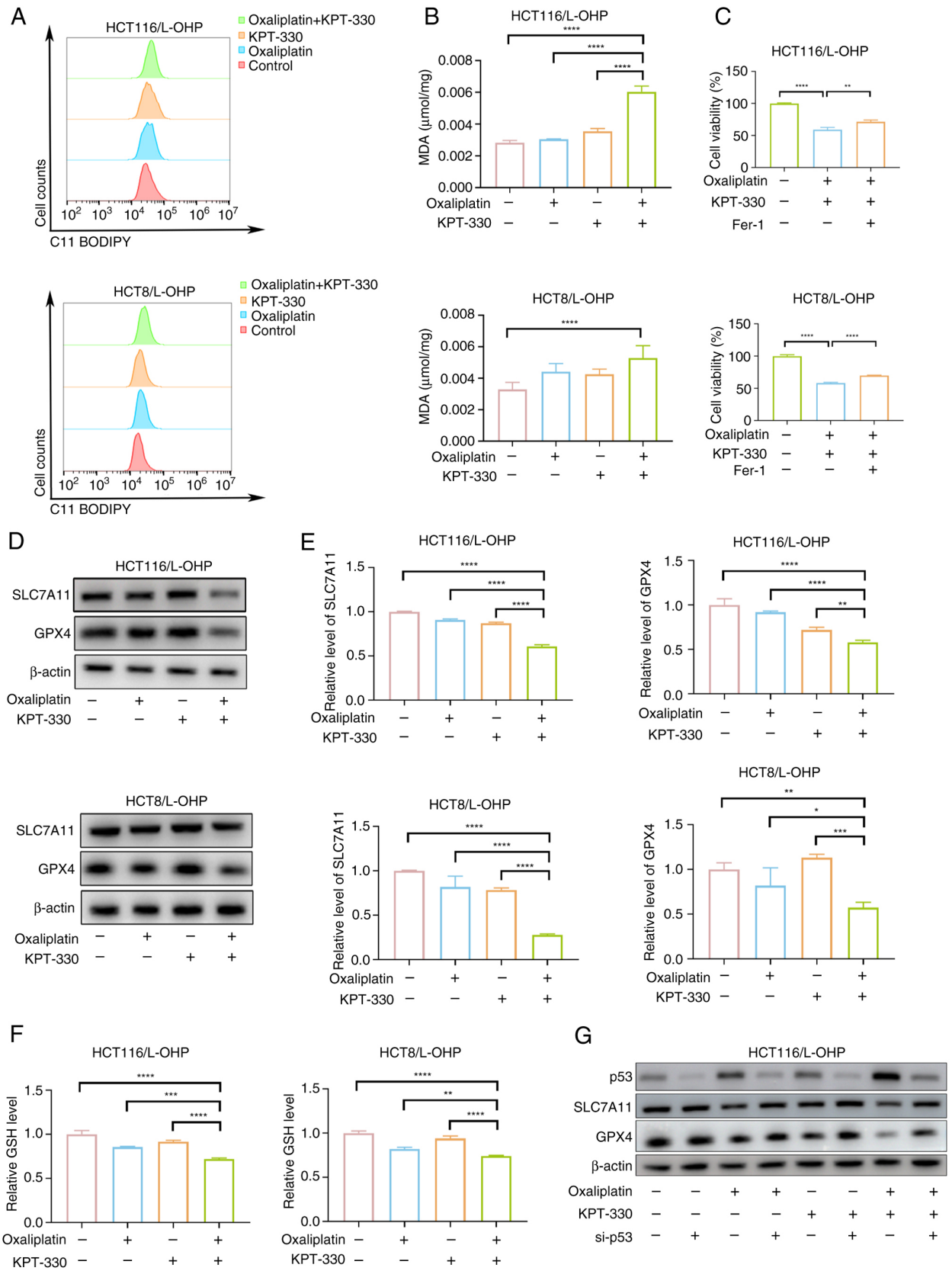

Figure 5. Combination of KPT-330 and oxaliplatin inhibits SLC7A11 and GPX4 expression to induce ferroptosis. (A) HCT116/L-OHP and HCT8/L-OHP cells were treated with oxaliplatin, KPT-330 or the combination for 48 h, stained with C11-BODIPY, and analyzed by flow cytometry. (B) MDA levels after treatment of HCT116/L-OHP and HCT8/L-OHP cells with oxaliplatin, KPT-330 or the combination for 48 h. (C) Viability of HCT116/L-OHP and HCT8/L-OHP cells treated with KPT-330 and oxaliplatin or the combination with Fer-1 for 48 h, analyzed using a Cell Counting Kit-8 assay. (D) Immunoblot analysis of HCT116/L-OHP and HCT8/L-OHP cells treated with oxaliplatin, KPT-330 or the combination for 48 h. (E) mRNA expression levels of SLC7A11 and GPX4 in HCT116/L-OHP and HCT8/L-OHP cells treated with oxaliplatin, KPT-330 or the combination for 48 h. (F) Relative GSH levels assessed after treating HCT116/L-OHP and HCT8/L-OHP cells with oxaliplatin, KPT-330 or the combination for 48 h. (G) Immunoblot analysis of HCT116/L-OHP cells after knockdown of p53, and treatment with oxaliplatin, KPT-330 or the combination for 48 h. *P<0.05, **P<0.01, ***P<0.001, ****P<0.0001. Fer-1, ferrostatin-1; GPX4, glutathione peroxidase 4; GSH, glutathione; MDA, malondialdehyde; si, small interfering RNA; SLC7A11, solute carrier family 7 member 11.

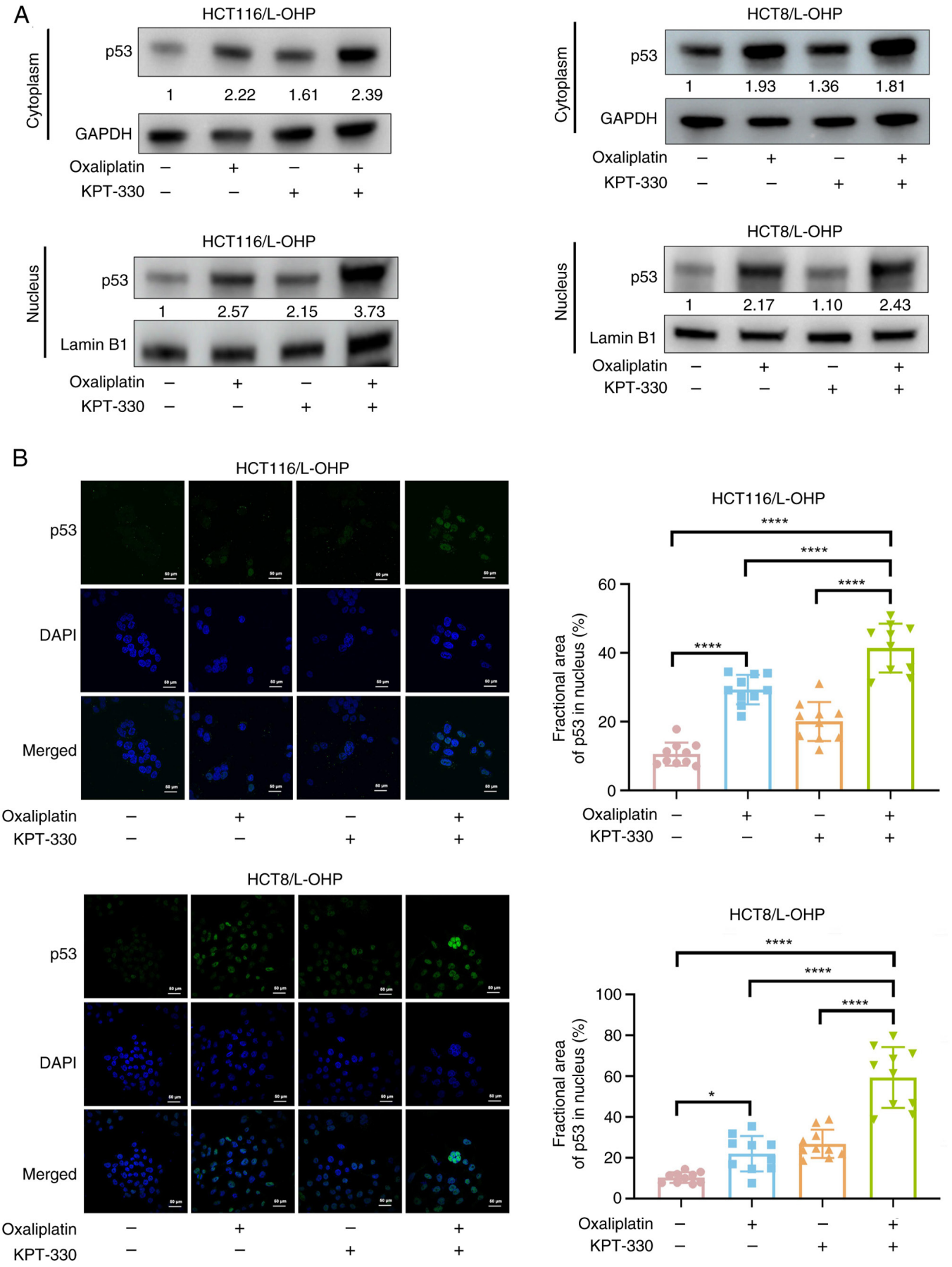

Figure 6. Combination of KPT-330 and oxaliplatin induces p53 nuclear retention. (A) HCT116/L-OHP and HCT8/L-OHP cells were treated with oxaliplatin, KPT-330 or the combination for 48 h, followed by collection of cytosolic and nuclear fractions for immunoblotting analysis. (B) HCT116/L-OHP and HCT8/L-OHP cells were treated with oxaliplatin, KPT-330 or the combination for 48 h, and then subjected to immunofluorescence staining. p53 localization was detected using an anti-p53 antibody, and nuclei were labeled with DAPI. *P<0.05; ****P<0.0001. Scale bar, 50 μm.

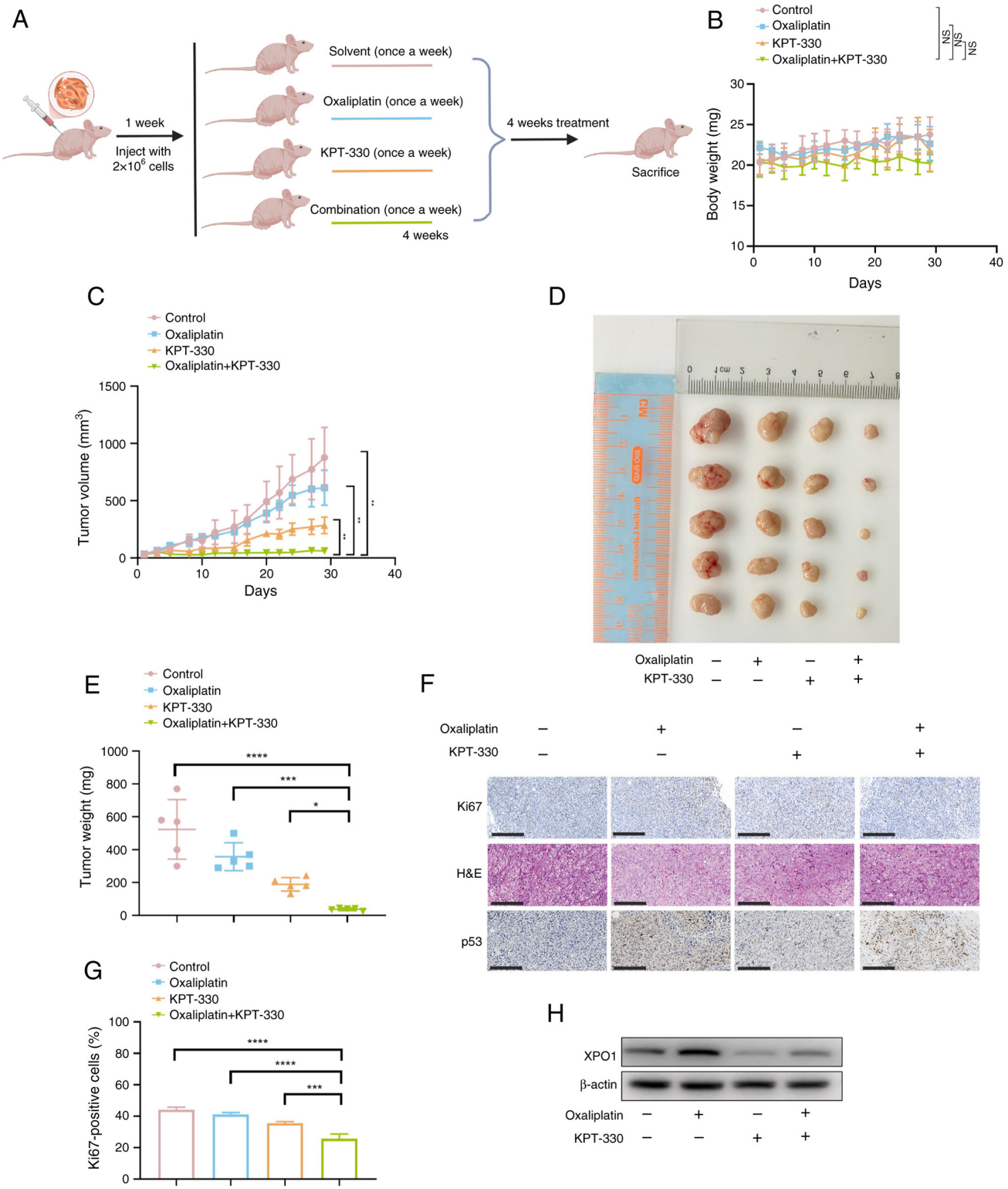

Figure 7. Combination of KPT-330 and oxaliplatin effectively suppresses tumor growth in a mouse xenograft model. (A) A subcutaneous tumor xenograft model was established by injecting HCT116/L-OHP cells into the subcutaneous tissue of nude mice. At 1 week after tumor establishment, four treatment groups were formed: Vehicle control, oxaliplatin, KPT-330 and combination. (B) Body weight curves of mice during the *in vivo* efficacy assessment of oxaliplatin and KPT-330 in HCT116/L-OHP xenografts. The NS symbol indicates that the weight in the combination therapy group was not significantly different from those in the single-drug (oxaliplatin or KPT-330) and vehicle control groups at the final timepoint. (C) Growth curve of tumor volume in the *in vivo* efficacy assessment of oxaliplatin and KPT-330 in HCT116/L-OHP xenografts. (D) Representative images of tumors from all groups (n=5). (E) Tumor weights in each group (n=5). (F) Representative staining images of Ki67, H&E and p53 in HCT116/L-OHP xenograft tumors. Scale bar, 50 μm. (G) Quantification of Ki67 in HCT116/L-OHP xenograft tumors treated with oxaliplatin, KPT-330 or the combination. (H) Immunoblot analysis of HCT116/L-OHP xenograft tumors treated with oxaliplatin, KPT-330 or the combination. *P<0.05, **P<0.01, ***P<0.001, ****P<0.0001. NS, not significant; XPO1, exportin 1.

group was not significantly different from those of the single-drug (oxaliplatin or KPT-330) and vehicle control groups (Fig. 7B). Additionally, after 4 weeks of treatment, the combination therapy group showed a significant reduction in

both tumor volume and mass compared with the monotherapy (oxaliplatin or KPT-330) and control groups (Fig. 7C-E), supporting the present *in vitro* findings. Further IHC staining revealed that the combination treatment reduced the proliferation index, as indicated by decreased Ki67 expression (Fig. 7F and G). Combination therapy with KPT-330 significantly enhanced the nuclear accumulation of p53, an effect that was only partially achieved with oxaliplatin treatment alone (Fig. 6A and B). IHC analysis of xenograft tumors revealed a similar trend, with the combination treatment promoting p53 accumulation, particularly in the nucleus (Fig. 7F). Additionally, western blot analysis revealed that oxaliplatin treatment increased XPO1 expression (Fig. 7H). These data demonstrated the effectiveness of the combination of oxaliplatin and KPT-330 in overcoming oxaliplatin resistance in CRC.

Discussion

Oxaliplatin is a widely used chemotherapeutic agent in the treatment of CRC (7). However, the development of resistance to oxaliplatin limits its clinical efficacy (30). This resistance is often associated with the adaptive tolerance of tumor cells to cell death mechanisms (31). Therefore, strategies aimed at enhancing tumor cell sensitivity to oxaliplatin are critical for developing effective approaches to overcome chemoresistance. In the present study, a mechanism was proposed to explain how KPT-330 overcomes oxaliplatin resistance. First, it was observed that oxaliplatin treatment alone increased the expression levels of XPO1, which in turn, enhanced the nuclear and cytoplasmic levels of p53. This mislocalization of p53 prevented it from performing its tumor-suppressing function in the nucleus, thereby reducing the sensitivity of the CRC cells to oxaliplatin. KPT-330 combined with oxaliplatin restored oxaliplatin sensitivity by promoting the nuclear localization of p53. As shown in our model, KPT-330 blocked the XPO1-mediated nuclear export of p53 by inhibiting XPO1, leading to its accumulation in the nucleus. The nuclear p53 then acts as a transcription factor, leading to the downregulation of SLC7A11 and the upregulation of p21. This, along with a decrease in MMP, collectively promotes both apoptosis and ferroptosis in the CRC cells, effectively overcoming oxaliplatin resistance (Fig. S5).

Several tumor suppressor proteins (TSPs), such as p53 and p21, are crucial for maintaining cellular integrity by regulating cell proliferation, apoptosis and DNA damage repair (32). Consequently, mislocalization of TSPs to the cytoplasm can contribute to tumor progression (33). One approach to prevent such mislocalization is to inhibit the nuclear export of these proteins (34). XPO1 serves as the sole nuclear export receptor for multiple TSPs (35). Upregulation of XPO1 expression has been linked to poor prognosis and chemoresistance in various cancer types, including breast cancer, CRC and leukemia (34-36). The XPO1 inhibitor KPT-330 induces nuclear accumulation of TSPs and restores their tumor-suppressive activity (14). In the present study, oxaliplatin not only increased XPO1 expression but also upregulated p53 expression in both the cytoplasm and nucleus in oxaliplatin-resistant cells. This suggests that targeting XPO1 could be a promising therapeutic strategy for cancer treatment.

In the cytoplasm, p53 is rapidly degraded via the ubiquitin-proteasome pathway, making it barely detectable (37). Maintaining p53 activity is a hallmark of sensitivity to oxaliplatin (38). p53 remains in the cytoplasm of platinum-resistant cells in lung and ovarian cancer (39,40). The mislocalization of p53 results in its inactivation, which is a critical factor in chemoresistance (41,42). In the present study, the combination of KPT-330 and oxaliplatin treatment increased p53 nuclear localization, downregulated SLC7A11 and GPX4 expression, and promoted ferroptosis compared with either oxaliplatin or KPT-330 monotherapy. Conversely, inhibition of p53 accumulation by transfection with si-p53 partially restored SLC7A11 and GPX4 expression. These results suggested that the detection of p53 nucleocytoplasmic localization could serve as a potential biomarker for predicting CRC response to oxaliplatin.

While the present study demonstrated the synergistic efficacy of KPT-330 and oxaliplatin in overcoming oxaliplatin resistance in CRC, several limitations remain. Direct validation of these findings in clinical samples from patients with CRC is essential. Additionally, the present study did not predict responsiveness based on p53 nucleocytoplasmic localization in relevant clinical samples. Future research will focus on analyzing XPO1 expression and p53 localization in patient tissues, particularly those from patients with CRC exhibiting oxaliplatin resistance, to confirm these results and further explore the translational potential of this combination therapy.

While the present *in vivo* experiments indicated no significant changes in body weight, suggesting a lack of acute severe toxicity during the treatment period, a thorough evaluation of the long-term safety and potential systemic side effects of combination therapy is crucial. Future research will focus on rigorous toxicology studies and comprehensive assessments of organ-specific toxicities, which are essential for its eventual clinical translation.

Furthermore, while the present study comprehensively outlined the role of the p53-XPO1 axis in the ability of KPT-330 to restore oxaliplatin sensitivity in CRC, the full range of the mechanistic actions of KPT-330 may extend beyond p53. Other factors contributing to increased cytoplasmic p53 levels, such as the ubiquitin-proteasome pathway and nuclear transport mechanisms, were not fully explored. For instance, impaired p53 nuclear import could contribute to its cytoplasmic retention (42). As a selective XPO1 inhibitor, KPT-330 may also affect the nuclear-cytoplasmic transport of other critical proteins, including additional tumor suppressors or factors (such as ERK5, DEAD-box helicase 17 and FOXO1) involved in drug resistance (33,43). Future investigations should explore these potential targets and alternative signaling pathways to gain a more comprehensive understanding of the multifaceted role of KPT-330 in overcoming oxaliplatin resistance.

In conclusion, KPT-330 promoted p53 nuclear accumulation and enhanced the sensitivity of oxaliplatin-resistant CRC to oxaliplatin. These findings suggest a promising strategy for overcoming oxaliplatin resistance in CRC and highlight the potential of KPT-330 as a novel sensitizing agent for this chemotherapy.

Acknowledgements

Not applicable.

Funding

The present study was supported by the National Natural Science Foundation of China (grant nos. 82072628 and 32200593), the Key Research and Development Program of Zhejiang (grant no. 2022C03032), and the Natural Science Foundation of Zhejiang Province, China (grant no. LQ23H160040).

Availability of data and materials

The data generated in the present study may be requested from the corresponding author.

Authors' contributions

CL, XJ, YC, KC, FW, QZ, XX, ZSC, LX and SD contributed to the conception and design of the study. CL, XJ, YC, KC, FW, QZ and XX contributed to data acquisition. CL, LX and SD contributed to data analysis and interpretation. CL and LX contributed to the writing of the original draft. SD and ZSC contributed to mentoring, writing, review and editing. CL, XJ and LX confirm the authenticity of all the raw data. All authors have read and approved the final version of the manuscript.

Ethics approval and consent to participate

Animal welfare and experimental procedures were carried out in accordance with the Guide for the Care and Use of Laboratory Animals and were approved by the Ethical Review Committee and Laboratory Animal Welfare Committee of the Sir Run Run Shaw Hospital, Zhejiang University School of Medicine (approval no. SRRSH2025-0023, Hangzhou, China).

Patient consent for publication

Not applicable.

Competing interests

The authors declare that they have no competing interests.

References

1. Sung H, Ferlay J, Siegel RL, Laversanne M, Soerjomataram I, Jemal A and Bray F: Global cancer statistics 2020: GLOBOCAN estimates of incidence and mortality worldwide for 36 cancers in 185 countries. CA Cancer J Clin 71: 209-249, 2021.
2. Cao W, Chen HD, Yu YW, Li N and Chen WQ: Changing profiles of cancer burden worldwide and in China: A secondary analysis of the global cancer statistics 2020. Chin Med J (Engl) 134: 783-791, 2021.
3. Bullock AJ, Schlechter BL, Fakih MG, Tsimberidou AM, Grossman JE, Gordon MS, Wilky BA, Pimentel A, Mahadevan D, Balmanoukian AS, *et al*: Botensilimab plus balstilimab in relapsed/refractory microsatellite stable metastatic colorectal cancer: A phase 1 trial. Nat Med 30: 2558-2567, 2024.
4. Tripathi PK, Mittal KR, Jain N, Sharma N and Jain CK: KRAS pathways: A potential gateway for cancer therapeutics and diagnostics. Recent Pat Anticancer Drug Discov 19: 268-279, 2024.
5. Capdevila J, Elez E, Peralta S, Macarulla T, Ramos FJ and Tabernero J: Oxaliplatin-based chemotherapy in the management of colorectal cancer. Expert Rev Anticancer Ther 8: 1223-1236, 2008.
6. Sargent D, Sobrero A, Grothey A, O'Connell MJ, Buyse M, Andre T, Zheng Y, Green E, Labianca R, O'Callaghan C, *et al*: Evidence for cure by adjuvant therapy in colon cancer: Observations based on individual patient data from 20,898 patients on 18 randomized trials. J Clin Oncol 27: 872-877, 2009.
7. Zeng K, Li W, Wang Y, Zhang Z, Zhang L, Zhang W, Xing Y and Zhou C: Inhibition of CDK1 overcomes oxaliplatin resistance by regulating ACSL4-mediated ferroptosis in colorectal cancer. Adv Sci (Weinh) 10: e2301088, 2023.
8. Li Y, Gan Y, Liu J, Li J, Zhou Z, Tian R, Sun R, Liu J, Xiao Q, Li Y, *et al*: Downregulation of MEIS1 mediated by ELFN1-AS1/EZH2/DNMT3a axis promotes tumorigenesis and oxaliplatin resistance in colorectal cancer. Signal Transduct Target Ther 7: 87, 2022.
9. Abdul Razak AR, Mau-Soerensen M, Gabrail NY, Gerecitano JF, Shields AF, Unger TJ, Saint-Martin JR, Carlson R, Landesman Y, McCauley D, *et al*: First-in-class, first-in-human phase I study of selinexor, a selective inhibitor of nuclear export, in patients with advanced solid tumors. J Clin Oncol 34: 4142-4150, 2016.
10. Ben-Barouch S and Kuruvilla J: Selinexor (KTP-330)-a selective inhibitor of nuclear export (SINE): Anti-tumor activity in diffuse large B-cell lymphoma (DLBCL). Expert Opin Investig Drugs 29: 15-21, 2020.
11. Ferreiro-Neira I, Torres NE, Liesenfeld LF, Chan CH, Penson T, Landesman Y, Senapedis W, Shacham S, Hong TS and Cusack JC: XPO1 inhibition enhances radiation response in preclinical models of rectal cancer. Clin Cancer Res 22: 1663-1673, 2016.
12. Inoue A, Robinson FS, Minelli R, Tomihara H, Rizi BS, Rose JL, Kodama T, Srinivasan S, Harris AL, Zuniga AM, *et al*: Sequential administration of XPO1 and ATR inhibitors enhances therapeutic response in TP53-mutated colorectal cancer. Gastroenterology 161: 196-210, 2021.
13. Quintanal-Villalonga A, Taniguchi H, Hao Y, Chow A, Zhan YA, Chavan SS, Uddin F, Allaj V, Manoj P, Shah NS, *et al*: Inhibition of XPO1 sensitizes small cell lung cancer to first- and second-line chemotherapy. Cancer Res 82: 472-483, 2022.
14. Chen Y, Camacho SC, Silvers TR, Razak AR, Gabrail NY, Gerecitano JF, Kalir E, Pereira E, Evans BR, Ramus SJ, *et al*: Inhibition of the nuclear export receptor XPO1 as a therapeutic target for platinum-resistant ovarian cancer. Clinical Cancer Research 23: 1552-1563, 2017.
15. Livak KJ and Schmittgen TD: Analysis of relative gene expression data using real-time quantitative PCR and the 2(-Delta Delta C(T)) method. Methods 25: 402-408, 2001.
16. Zhou J, Lei Z, Chen J, Liao S, Chen Y, Liu C, Huang S, Li L, Zhang Y, Wang P, *et al*: Nuclear export of BATF2 enhances colorectal cancer proliferation through binding to CRM1. Clin Transl Med 13: e1260, 2023.
17. Azmi AS, Kauffman M, McCauley D, Shacham S and Mohammad RM: Novel small-molecule CRM-1 inhibitor for GI cancer therapy. J Clin Oncol 30 (suppl 4): abstr 245, 2012.
18. Chiu SJ, Lee YJ, Hsu TS and Chen WS: Oxaliplatin-induced gamma-H2AX activation via both p53-dependent and -independent pathways but is not associated with cell cycle arrest in human colorectal cancer cells. Chem Biol Interact 182: 173-182, 2009.
19. Schmidt AK, Pudelko K, Boekenkamp JE, Berger K, Kschischo M and Bastians H: The p53/p73-p21(CIP1) tumor suppressor axis guards against chromosomal instability by restraining CDK1 in human cancer cells. Oncogene 40: 436-451, 2021.
20. Martinez-Balibrea E, Martinez-Cardus A, Gines A, Ruiz de Porras V, Moutinho C, Layos L, Manzano JL, Bugés C, Bystrup S, Esteller M and Abad A: Tumor-related molecular mechanisms of oxaliplatin resistance. Mol Cancer Ther 14: 1767-1776, 2015.
21. Yapasert R, Khaw-On P and Banjerdpongchai R: Coronavirus Infection-associated cell death signaling and potential therapeutic targets. Molecules 26: 7459, 2021.
22. Arango D, Wilson AJ, Shi Q, Corner GA, Arañes MJ, Nicholas C, Lesser M, Mariadason JM and Augenlicht LH: Molecular mechanisms of action and prediction of response to oxaliplatin in colorectal cancer cells. Br J Cancer 91: 1931-1946, 2004.
23. Xu X, Lai Y and Hua ZC: Apoptosis and apoptotic body: Disease message and therapeutic target potentials. Biosci Rep 39: BSR20180992, 2019.

24. Stockwell BR, Friedmann Angeli JP, Bayir H, Bush AI, Conrad M, Dixon SJ, Fulda S, Gascón S, Hatzios SK, Kagan VE, *et al*: Ferroptosis: A regulated cell death nexus linking metabolism, redox biology, and disease. Cell 171: 273-285, 2017.
25. Yang C, Zhang Y, Lin S, Liu Y and Li W: Suppressing the KIF20A/NUAK1/Nrf2/GPX4 signaling pathway induces ferroptosis and enhances the sensitivity of colorectal cancer to oxaliplatin. Aging (Albany NY) 13: 13515-13534, 2021.
26. Lin JF, Hu PS, Wang YY, Tan YT, Yu K, Liao K, Wu QN, Li T, Meng Q, Lin JZ, *et al*: Phosphorylated NFS1 weakens oxaliplatin-based chemosensitivity of colorectal cancer by preventing PANoptosis. Signal Transduct Target Ther 7: 54, 2022.
27. Di Y, Zhang X, Wen X, Qin J, Ye L, Wang Y, Song M, Wang Z and He W: MAPK Signaling-mediated RFNG phosphorylation and nuclear translocation restrain oxaliplatin-induced apoptosis and ferroptosis. Adv Sci (Weinh) 11: e2402795, 2024.
28. Wang Z, Zhan Y, Xu J, Wang Y, Sun M, Chen J, Liang T, Wu L and Xu K: β-Sitosterol reverses multidrug resistance via BCRP suppression by inhibiting the p53-MDM2 interaction in colorectal cancer. J Agric Food Chem 68: 3850-3858, 2020.
29. O'Brate A and Giannakakou P: The importance of p53 location: Nuclear or cytoplasmic zip code? Drug Resist Updat 6: 313-322, 2003.
30. Kanemitsu Y, Shimizu Y, Mizusawa J, Inaba Y, Hamaguchi T, Shida D, Ohue M, Komori K, Shiomi A, Shiozawa M, *et al*: Hepatectomy followed by mFOLFOX6 versus hepatectomy alone for liver-only metastatic colorectal cancer (JCOG0603): A phase II or III randomized controlled trial. J Clin Oncol 39: 3789-3799, 2021.
31. Luo S, Yue M, Wang D, Lu Y, Wu Q and Jiang J: Breaking the barrier: Epigenetic strategies to combat platinum resistance in colorectal cancer. Drug Resist Updat 77: 101152, 2024.
32. Kau TR, Way JC and Silver PA: Nuclear transport and cancer: From mechanism to intervention. Nat Rev Cancer 4: 106-117, 2004.
33. Lai C, Xu L and Dai S: The nuclear export protein exportin-1 in solid malignant tumours: From biology to clinical trials. Clin Transl Med 14: e1684, 2024.
34. Turner JG, Dawson JL, Grant S, Shain KH, Dalton WS, Dai Y, Meads M, Baz R, Kauffman M, Shacham S and Sullivan DM: Treatment of acquired drug resistance in multiple myeloma by combination therapy with XPO1 and topoisomerase II inhibitors. J Hematol Oncol 9: 73, 2016.
35. Saenz-Ponce N, Pillay R, de Long LM, Kashyap T, Argueta C, Landesman Y, Hazar-Rethinam M, Boros S, Panizza B, Jacquemyn M, *et al*: Targeting the XPO1-dependent nuclear export of E2F7 reverses anthracycline resistance in head and neck squamous cell carcinomas. Sci Transl Med 10: eaar7223, 2018.
36. Kim J, McMillan E, Kim HS, Venkateswaran N, Makkar G, Rodriguez-Canales J, Villalobos P, Neggers JE, Mendiratta S, Wei S, *et al*: XPO1-dependent nuclear export is a druggable vulnerability in-mutant lung cancer. Nature 538: 114-117, 2016.
37. Oren M and Rotter V: Mutant p53 gain-of-function in cancer. Cold Spring Harb Perspect Biol 2: a001107, 2010.
38. Toscano F, Parmentier B, Fajoui ZE, Estornes Y, Chayvialle JA, Saurin JC and Abello J: p53 dependent and independent sensitivity to oxaliplatin of colon cancer cells. Biochem Pharmacol 74: 392-406, 2007.
39. Nishitsuji K, Mito R, Ikezaki M, Yano H, Fujiwara Y, Matsubara E, Nishikawa T, Ihara Y, Uchimura K, Iwahashi N, *et al*: Impacts of cytoplasmic p53 aggregates on the prognosis and the transcriptome in lung squamous cell carcinoma. Cancer Sci 115: 2947-2960, 2024.
40. Komlodi-Pasztor E, Trostel S, Sackett D, Poruchynsky M and Fojo T: Impaired p53 binding to importin: A novel mechanism of cytoplasmic sequestration identified in oxaliplatin-resistant cells. Oncogene 28: 3111-3120, 2009.
41. Prokocimer M and Peller S: Cytoplasmic sequestration of wild-type p53 in a patient with therapy-related resistant AML: First report. Med Oncol 29: 1148-1150, 2012.
42. Fang J, Zou M, Yang M, Cui Y, Pu R and Yang Y: TAF15 inhibits p53 nucleus translocation and promotes HCC cell 5-FU resistance via post-transcriptional regulation of UBE2N. J Physiol Biochem 80: 919-933, 2024.
43. Wang Z, Pan B, Yao Y, Qiu J, Zhang X, Wu X and Tang N: XPO1 intensifies sorafenib resistance by stabilizing acetylation of NPM1 and enhancing epithelial-mesenchymal transition in hepatocellular carcinoma. Biomed Pharmacother 160: 114402, 2023.